Interphase precipitation in Ti–Nb and Ti–Nb–Mo bearing steel

J. H. Jang[1], Y.-U. Heo[1], C.-H. Lee[2], H. K. D. H. Bhadeshia[1,3] and Dong-Woo Suh*[1]

The interphase precipitation of carbides has been studied in two microalloyed steels containing Ti and Nb, but only one of which contains molybdenum. The precipitates obtained are, therefore, (Ti,Nb)C and (Ti,Nb,Mo)C respectively. It is found that molybdenum significantly reduces the size of the carbide precipitates and also strongly retards their coarsening behaviour during subsequent heat treatment. This is because it enhances the nucleation rate by reducing the interfacial energy, but it is not thermodynamically favoured within the (Ti,Nb,Mo)C, so the later stages of growth involve its partitioning into the matrix, thus explaining the reduction in coarsening rate relative to the molybdenum free steel.

Keywords: HSLA steel, TiC, Molybdenum, Niobium, Microstructure, Interphase precipitation

Introduction

Ferrite in the form of allotriomorphs and idiomorphs is the dominant phase in the vast majority of more than a billion tonnes of steel manufactured annually. With appropriate alloying, it becomes possible to observe a phenomenon known as interphase precipitation, in which particles of a third phase precipitate at an advancing α/γ interface.[1–4] This precipitate phase may be cementite, alloy carbides or other phases that have limited solubility in the majority phases at the transformation temperature. Examples include V_4C_3,[2,5–7] NbC,[1] $Cr_{23}C_6$,[8] and TiC.[9]

The characterisitic feature of interphase precipitation is the fine dispersion of precipitate particles observed as regular rows in thin foils examined using transmission electron microscopy (TEM), all of which usually have the same crystallographic orientation in any given ferrite grain. The process is for the most part associated with a mechanism in which the α/γ interface is translated by the propagation of steps, with the particles precipitating on the stationary, immobile component of the interface[8] because the steps themselves move too rapidly to allow successful nuclei to develop.[10,11]

The idea of interphase precipitation has been around for four decades, but remarkably, there have been new developments in the context of high strength low alloy steels used in structural applications with a yield strength in the range of 400–500 MPa.[12–14] The process involves the introduction of minute particles of TiC or (Ti,Mo)C particles, which result in the yield strength being elevated to $\simeq 780$ MPa while maintaining an elongation of some 20%. Typical compositions (wt-%) of such steels are in the range[12]

$$Fe - 0{\cdot}04C - 0{\cdot}2Si - 1{\cdot}5Mn - (0{\cdot}02 - 0{\cdot}2)Ti - (0 - 0{\cdot}4)Mo$$

Aspects of such steels are covered in Ref. 15 and further details in an article by Dunne.[16] Some variants also contain Nb,[17,18] and carbides of (Ti,Nb) and (Ti,Mo) have been found to induce significant precipitation hardening.[14] Recent work has explained the fundamental basis for the influence of molybdenum in suppressing the coarsening of the interphase precipitated carbides,[19] so the purpose of the present work was to examine the interphase precipitation behaviour of (Ti,Nb,Mo)C during isothermal treatment.

Experimental

Table 1 shows the chemical compositions of the experimental alloys studied.

Ingots 30 kg in weight were prepared by vacuum induction melting and reheated to 1200°C for hot rolling to 20 mm thick plates with a finishing temperature >900°C. Cylindrical specimens of diameters 8 and 12 mm long were then prepared and subjected to the heat treatment cycle illustrated in Fig. 1 using a thermomechanical simulator in order to stimulate interphase precipitation of the appropriate carbides. The specimens were heated to 1250°C for 300 s in vacuum to dissolve preexisting precipitates followed by hot compression at 1100 and 1000°C at a strain rate of 1 s^{-1} with total amount of strain of 0·3 to control the austenite grain size. After cooling to an isothermal temperature of 700°C, the specimens were held for 40 min before final cooling to room temperature. Two prolonged aging treatments were additionally conducted to investigate the coarsening of carbides, where the specimens were encapsulated in evacuated quartz tubes and held for 24 and 120 h at 650 and 700°C respectively.

Longitudinal sections etched using 2% nital were observed using light microscopy with higher resolution

---

[1]Graduate Institute of Ferrous Technology, Pohang University of Science and Technology, Pohang 790-784, Korea
[2]Technical Research Laboratories, POSCO, Pohang 790-785, Korea
[3]Materials Science and Metallurgy, University of Cambridge, UK

*Corresponding author, email dongwoo1@postech.ac.kr
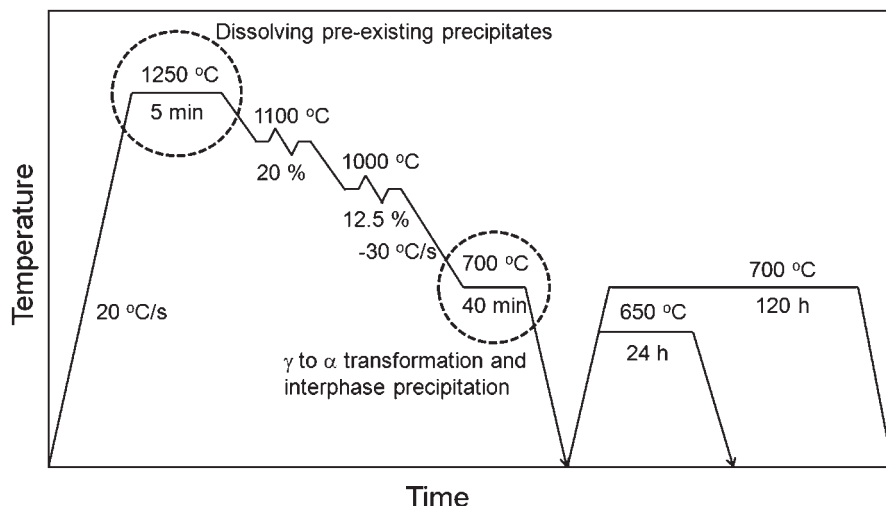
1 Schematic representation of heat treatment

observations made using a TEM equipped with a field emission gun operated at 200 kV, together with energy dispersive X-ray spectroscopy (EDS). Thin foil samples were prepared by mechanically thinning samples to 0·08 mm by abrasion on SiC papers and then electro-polishing using a mixture of 5% perchloric acid and 95% ethanol at 18°C with a current of 60–70 mA. Carbon extraction replicas were also prepared by depositing carbon on the etched specimen, followed by electro-polishing using a mixture of 10% perchloric acid and 90% ethanol at room temperature with 0·015 mA until the replicas began to lift for collection on a copper support grid.

The fraction of ferrite was measured from optical micrographs, and the precipitate sizes determined from the TEM images, in both cases using image analysis software. The particle radius was estimated as the maximum distance from its centre. The carbide composition was characterised using EDS on thin foil samples or on carbon extraction replicas. It is fortunate that there is no overlap of information from the matrix in the thin foil samples because the concentrations of Ti, Nb and Mo in the ferrite are extremely small.

The hardness of ferrite was determined using a Vickers tester with a load of just 1 kg in order to avoid interference from the low temperature transformation products. The results were averaged over 30 sampling points.

Results and discussion

Figure 2 presents optical micrographs of Ti–Nb and Ti–Nb–Mo steels after isothermal treatment at 700°C for 40 min, illustrating the allotriomorphic ferrite and the darker martensite that forms during cooling to ambient temperature. The volume fraction of ferrite is evaluated to be 0·72±0·05 for both alloys. The ferrite grain size was ~25±5 μm, and no significant difference was observed depending on the molybdenum addition.

Table 1 Alloy compositions (wt-%)

	C	Mn	Ti	Nb	Mo	Al
Ti–Nb	0·071	1·76	0·094	0·030	…	0·026
Ti–Nb–Mo	0·067	1·78	0·095	0·030	0·200	0·028

Figure 3*a* and *c* shows dark field images of carbides in Ti–Nb steels after isothermal treatment at 700°C for 40 min and after the prolonged aging at 650°C for 24 h. Carbide distribution after aging at 700°C for 120 h is also shown in Fig. 3*d* using a carbon extraction replica. The dark field images obtained with [012] zone axis of ferrite show carbides as rows, consistent with interphase precipitation. In isothermally heat treated specimen at 700°C for 40 min, the carbides in Ti–Nb steel show curved rows of precipitates with irregular spacing. The average distance is about 40–45 nm; given this fine spacing, it is known that the row structure can only be resolved if the precipitation planes are parallel to the beam direction;[20] therefore, it can be concluded that the precipitation plane in Fig. 3*a* is roughly parallel to the $(0\bar{2}1)$ plane of ferrite matrix. The particle radius is 4·1±1·8 nm after isothermal treatment for 40 min and increases to 5·7±2·8 and 7·6±4·2 nm after aging for 24 and 120 h respectively.

Corresponding TEM images of carbides in Ti–Nb–Mo steel are shown in Fig. 4. The dark field images of carbide obtained also with the [012] zone axis of ferrite show much more planar interphase precipitation with regular spacing of 22 nm, which is about a half of that in Ti–Nb steel. The particle radius is 2·8±2·5, 2·8±1·8 and 4·3±3·1 nm after 40 min, 24 h and 120 h aging respectively, indicating refinement of carbide size and the coarsening rate reduced by the Mo addition.

Analyses of Ti, Nb and Mo contents in the carbide for the specimen aging for 120 h are shown in Table 2. It is evident that the coarsening carbides contain less Mo than during the early stages of precipitation. The molybdenum addition nevertheless reduces the row spacing and the size of the interphase precipitates. Molybdenum may therefore be interpreted as having a beneficial effect in reducing the length scales associated with precipitation at the austenite/ferrite interface and subsequent coarsening after the passage of the transformation interface.

Most alloying additions with the exception of cobalt and aluminium retard the transformation of austenite into ferrite by increasing the relative thermodynamic stability of the austenite. Given this thermodynamic effect, both the nucleation and the rate of interface motion may be retarded. In the Ti–Nb–Mo steel, even though a portion of the Mo atoms is consumed by the formation of
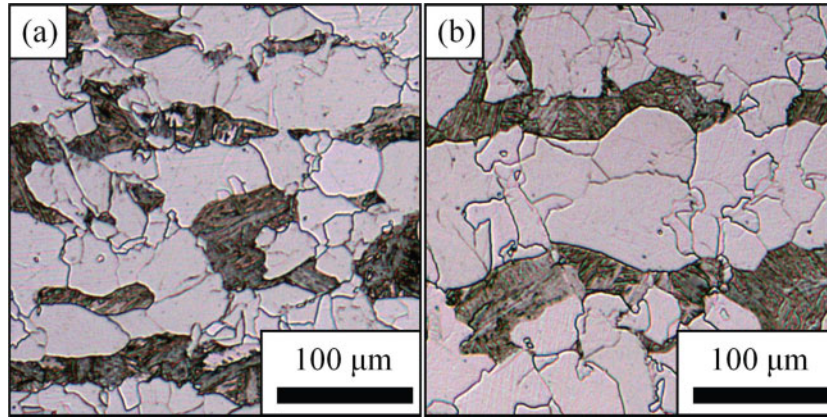
2 Optical micrographs of *a* Ti–Nb and *b* Ti–Nb–Mo steels after isothermal treatment at 700°C for 40 min

(Ti,Nb,Mo)C carbide, molybdenum dissolved in the austenite is likely to influence on the transformation kinetics. Figure 5 shows the dilatation curves of Ti–Nb and Ti–Nb–Mo steel during the isothermal treatment at 700°C in Fig. 1. As expected, the rate of overall transformation is reduced by the molybdenum addition. This is consistent with the fact that molybdenum is well known to reduce the magnitude of $\Delta G^{\gamma\alpha} = G^{\alpha} - G^{\gamma}$ and $\Delta G^{\gamma(\alpha+\gamma'+\rho)} = (G^{\alpha} + G^{\gamma'} + G^{\rho}) - G^{\gamma}$, where G represents the Gibbs free energy of the phase concerned and the superscript ρ represents the carbide. These values were calculated using ThermoCalc with the TCFE6·2 database for 700°C. The $\Delta G^{\gamma\alpha}$ values are $-230\cdot5$ and $-157\cdot5$ J mol^{-1} for Ti–Nb and Ti–Nb–Mo respectively.

The $\Delta G^{\gamma(\alpha+\gamma+\rho)}$ are $-335\cdot5$ and $-246\cdot9$ J mol^{-1} for Ti–Nb and Ti–Nb–Mo respectively. It is noted that the $\Delta G^{\gamma(\alpha+\gamma'+\rho)}$ is larger magnitude than $\Delta G^{\gamma\alpha}$ in both alloys because the formation of the carbide makes the system more stable. Molybdenum clearly reduces the driving force available for transformation in both scenarios.

It remains to explain why the precipitate size and row spacing are smaller in the Ti–Mo–Nb system. There are three models in the literature for the calculation of row spacing. The first[21] focuses on the nucleation of super-ledges at the ferrite/austenite interface and has been shown to correctly predict the minimum row spacings to be expected as a function of $\Delta G^{\gamma\alpha}$. The row spacing is predicted to decrease as the driving force is increased,
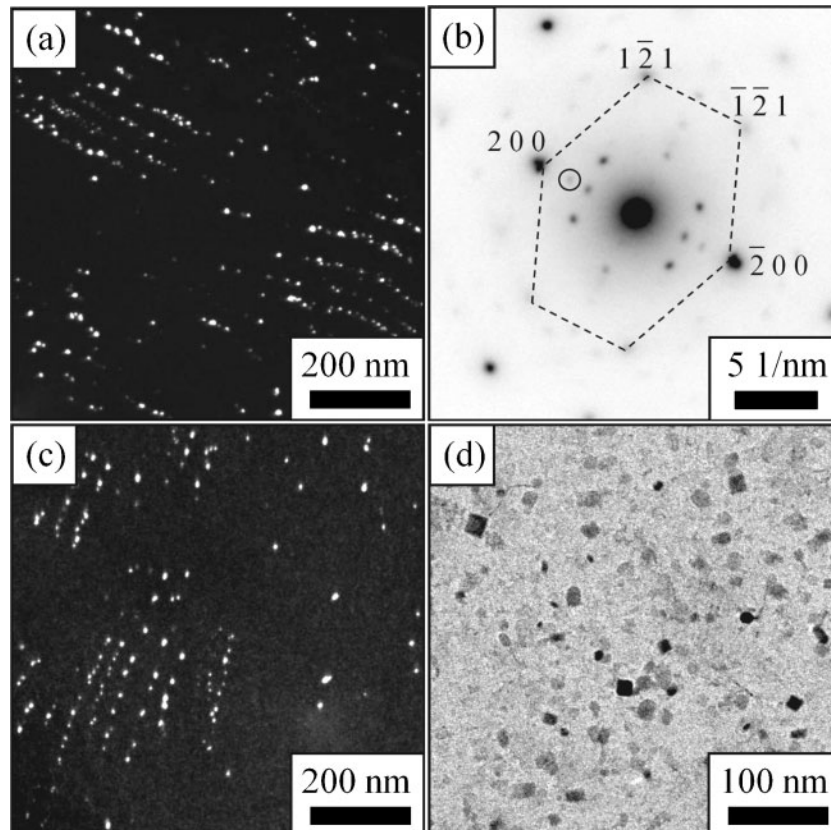
a dark field image after isothermal treatment at 700°C for 40 min and *b* its corresponding diffraction pattern; *c* dark field image after prolonged aging at 650°C for 24 h; *d* carbon replication image after prolonged aging at 700°C for 120 h
3 Images (TEM) of Ti–Nb steel
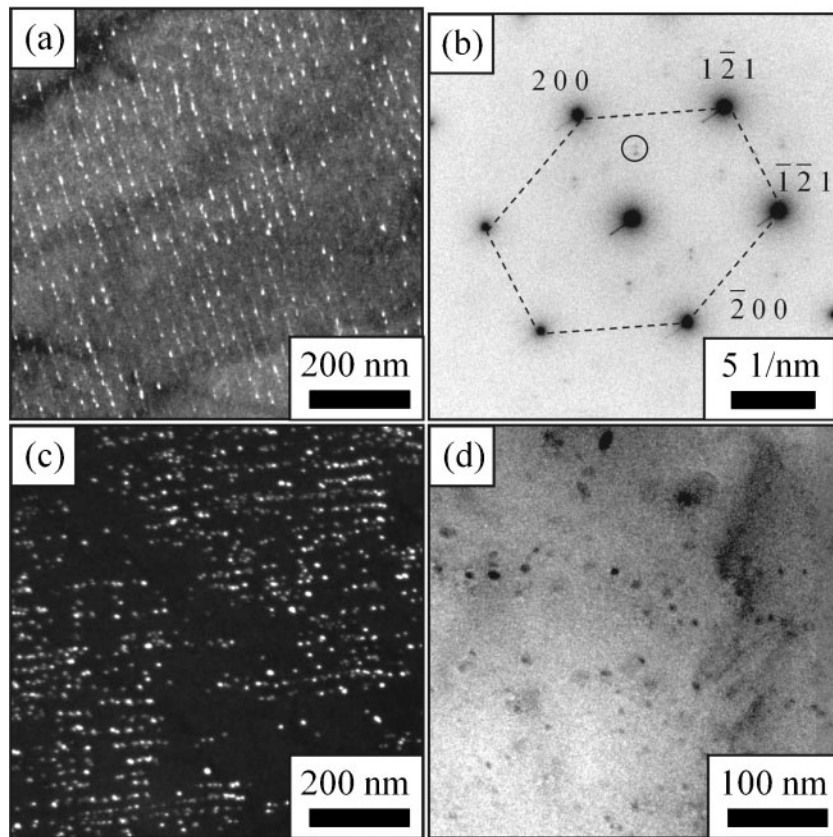
a dark field image after isothermal treatment at 700°C for 40 min and *b* its corresponding diffraction pattern; *c* dark field image after prolonged aging at 650°C for 24 h; *d* carbon replication image after prolonged aging at 700°C for 120 h

4 Images (TEM) of Ti–Nb–Mo steel

and hence, this model cannot explain why the spacing is finer in the case of the Ti–Nb–Mo system where the driving force is in fact smaller.

The other two models[22,23] focus on the nucleation of the carbide determining the sheet spacing. However, they require the driving force for carbide nucleation to be greater in the Ti–Nb–Mo alloy compared with the Ti–Nb alloy. In contradiction, it has been established that the substitution of Mo into TiC is thermodynamically unfavourable.[19] We also note that none of the theories[21–23] explicitly account for the role of the alloying elements on the interfacial energy between the carbide and the major phases, a factor that has a profound effect on the activation energy for nucleation.

In turns out that the explanation for the observed effect of molybdenum is quite simple: recent work[19] has established, using both first principles calculations and detailed validation, that the partial substitution of Ti by Mo into TiC carbide is unfavourable with respect to the formation energy. However, there is a kinetic advantage
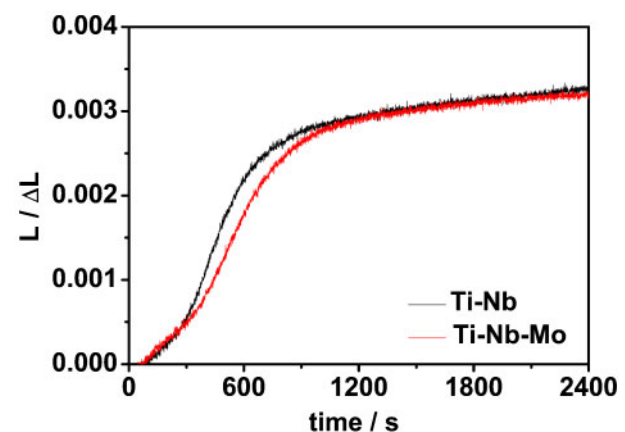
in incorporating molybdenum into the early stages of carbide formation because it has been shown to mitigate the misfit strain between the carbide and ferrite matrix, which is a huge advantage when the surface/volume ratio of the particle is large.[19] The later growth of the precipitate can occur without the presence of molybdenum, as indeed is observed here and in previous work.[19]

Finally, the difference in coarsening behaviour can be understood simply from the fact that the partitioning of the molybdenum accompanying the coarsening as (Ti,Nb)C during the prolonged aging in the Ti–Nb–Mo alloy would slow the rate relative to the case where the alloy does not contain any molybdenum.

Table 2 Particle sizes and solute concentrations in Ti, Nb and Mo carbide*

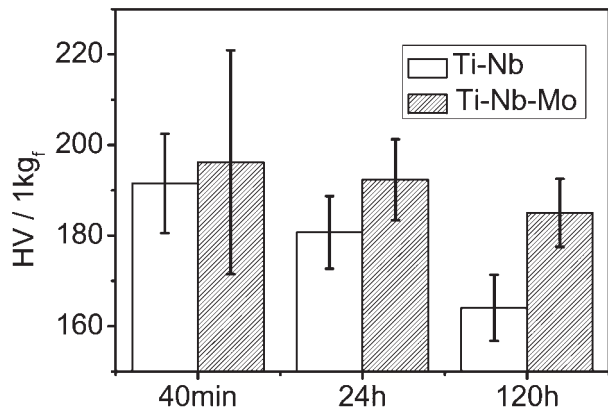| Particle size/nm	wt-%			at.-%		
	Ti	Nb	Mo	Ti	Nb	Mo
3–6	36±3·0	19±3·4	45±3·7	53	14	33
≥30	65±7·1	14±6·2	21±6·5	78	9	12

*Note that the presence of carbon is neglected in presenting these data since it could not be quantitatively analysed using EDS.

5 Dilatation curves of Ti–Nb and Ti–Nb–Mo steels during isothermal treatment at 700°C for 40 min

6 Hardness as function of aging period

Figure 6 shows the change of hardness with the Mo addition and aging time. Considering that the solid solution hardening effect of Mo is insignificant,[4] the difference in hardness is thought to be due primarily to the precipitation and coarsening behaviours of the carbide particles. After short isothermal treatment for 40 min, the hardness of Ti–Nb and Ti–Nb–Mo steels is 191 and 196 HV respectively. The corresponding hardness for the Ti–Nb alloy after prolonged aging for 24 and 120 h decreases to 181 and 164 HV, and those for Ti–Nb–Mo alloy is measured to be 192 and 185 HV respectively. The hardness of the Ti–Nb steel clearly decreases more rapidly than that of the Ti–Nb–Mo steels during prolonged aging. This indicates that even with an influence of Mo on the interphase precipitation behaviour of (Ti,Nb,Mo)C carbide by changing the morphology and row spacing, its effect on strength of ferrite is more pronounced during the coarsening stage, so that the role of Mo is identified as the suppression of that stage.

Conclusions

Two low alloy steels which differed only in the concentration of molybdenum have been studied. An examination of the interphase precipitation of (Ti,Nb)C and (Ti,Nb,Mo)C particles as a consequence of the stepwise translation of the ferrite/austenite interface revealed that the latter precipitates are significantly finer, as is the spacing between the rows of precipitates. The presence of molybdenum also significantly retards the subsequent coarsening behaviour of the carbide particles. It is also found that the molybdenum only participates as a constituent of the (Ti,Nb,Mo)C during the early stages of precipitation; the subsequent growth of the carbides occurs essentially as (Ti,Nb)C.

These results are consistent with previous research, which established that molybdenum is not thermodynamically favoured as a solute within TiC but nevertheless reduces the lattice misfit between the carbide and ferrite, thus making the nucleation process easier. The role of molybdenum is therefore to accelerate nucleation and hence lead to finer length scales during interphase precipitation. In the context of growth and coarsening, molybdenum retards both these processes by requiring that it partitions into the matrix since its presence is not favoured within the carbide.

References

1. J. M. Gray and R. B. G. Yeo: 'Niobium carbonitride precipitation in low-alloy steels with particular emphasis on precipitate-row formation', *Trans. ASM*, 1968, **61**, 255–269.
2. A. T. Davenport, F. G. Berry and R. W. K. Honeycombe: 'Interphase precipitation in iron alloys', *Met. Sci.*, 1968, **2**, 104–106.
3. R. W. K. Honeycombe: 'Ferrite', *Met. Sci.*, 1980, **14**, 201–214.
4. T. Gladman: 'The physical metallurgy of microalloyed steels'; 1996, London, IOM Communications.
5. A. D. Batte and R. W. K. Honeycombe: 'Strengthening of ferrite by vanadium carbide precipitation', *Met. Sci.*, 1973, **7**, 160–168.
6. G. L. Dunlop and R. W. K. Honeycombe: 'Ferrite morphologies and carbide precipitation in a Cr–Mo–V creep-resisting steel', *Met. Sci.*, 1976, **10**, 124–132.
7. A. Warren, H. S. Ubhi and D. H. Jack: 'Relationship between processing, microstructure and properties in controlled rolled 0·45% V steel', *Met. Sci.*, 1983, **17**, 19–26.
8. K. Campbell and R. W. K. Honeycombe: 'The isothermal decomposition of austenite in simple chromium steels', *Met. Sci.*, 1974, **8**, 197–203.
9. S. Freeman and R. W. K. Honeycombe: 'Strengthening of titanium steels by carbide precipitation', *Met. Sci.*, 1977, **11**, 59–64.
10. R. W. K. Honeycombe: 'Transformation from austenite in alloy steels', *Metall. Trans. A*, 1976, **7A**, 915–936.
11. H. I. Aaronson, M. R. Plichta, G. W. Franti and K. C. Russell: 'Precipitation at interphase boundaries', *Metall. Trans. A*, 1978, **9A**, 363–371.
12. Y. Funakawa, T. Shiozaki, K. Tomita, Y. Yamamoto and E. Maeda: 'Development of high strength hot-rolled sheet steel consisting of ferrite and nanometer-sized carbides', *ISIJ Int.*, 2004, **44**, 1945–1951.
13. K. Seto, Y. Funakawa and S. Kaneko: 'Hot rolled high strength steels for suspension and chassis parts "Nanohiten" and BHT steel', *JFE GIHO*, 2007, (16), 28–33.
14. C. Y. Chen, H. W. Yen, F. H. Kao, W. C. Li, C. Y. Huang, J. R. Yang and S. H. Wang: 'Precipitation hardening of high-strength low-alloy steels by nanometer-sized carbides', *Mater. Sci. Eng. A*, 2009, **A499**, 162–166.
15. H. W. Yen, C. Y. Chen, T. Y. Wang, C. Y. Huang and J. R. Yang: 'Orientation relationship transition of interphase-precipitated nanometer-sized TiC carbides in a Ti-bearing steel', *Mater. Sci. Technol.*, 2010, **26**, 421–430.
16. D. P. Dunne: 'Interaction of precipitation with recrystallisation and phase transformation in low alloy steels', *Mater. Sci. Technol.*, 2010, **26**, 410–420.
17. R. D. K. Misra, H. Nathani, J. E. Hartmann and F. Siciliano: 'Microstructural evolution in a new 770 MPa hot rolled Nb–Ti microalloyed steel', *Mater. Sci. Eng. A*, 2005, **A394**, 339–352.
18. B. Dutta, E. J. Palmiere and C. M. Sellars: 'Modelling the kinetics of strain induced precipitation in Nb microalloyed steels', *Acta Mater.*, 2001, **49**, 785–794.
19. J. H. Jang, C. H. Lee, Y. U. Heo and D. W. Suh: 'Stability of (Ti, M) C (M=Nb, V, Mo and W) carbide in steels using first-principles calculations', *Acta Mater.*, 2012, **60**, 208–217.
20. A. T. Davenport and R. W. K. Honeycombe: 'Precipitaiton of carbides at γ–α boundaries in alloy steels', *Proc. R. Soc. Lond. A*, 1971, **322A**, 191–205.
21. H. K. D. H. Bhadeshia: 'Diffusional transformations: the nucleation of superledges', *Phys. Status Solidi A*, 1982, **69A**, 745–750.
22. J. A. Todd, P. Li and S. M. Copley: 'A new model for precipitation at moving interphase boundaries', *Metall. Mater. Trans. A*, 1988, **19A**, 2133–2138.
23. R. Lagneborg and S. Zajac: 'Model for interphase precipitation of V-microalloyed structural steels', *Metall. Mater. Trans. A*, 2000, **31A**, 1–12.